

Open charm production at HERA

U. Karshon^a

^aWeizmann Institute of Science, Rehovot, Israel
On behalf of the H1 and ZEUS Collaborations

Inclusive charm meson production cross sections in the deep inelastic scattering and photoproduction regimes are compared with QCD leading and next-to-leading order (NLO) calculations. The NLO predictions are significantly below the data in some parts of the measured kinematic range. Angular distributions of dijet events with charm show clear evidence for the existence of charm originating from the incoming photon. The charm fragmentation function is measured for the first time at HERA. Various fragmentation ratios and the fragmentation fractions of the low-lying charm hadrons are determined and compared to previous e^+e^- results.

1. Introduction

During 1996–2000 HERA collided electrons or positrons ($E_e = 27.6$ GeV) with protons (E_p between 820 and 920 GeV). Open charm (c) production, which has been extensively studied, occurs in few steps: a) Hard process, e.g. boson-gluon fusion (BGF), where a photon (γ) or Z boson emitted from the incoming electron fuses with a gluon (g) from the proton, producing a cc pair; b) Initial/final state parton shower development; c) Fragmentation of a final-state parton into a hadron. Two kinematic regions have been explored: 1) Deep inelastic scattering (DIS) with photon virtuality $Q^2 > 1$ GeV², where the scattered electron is visible in the main detector; 2) Photoproduction (PHP) with $\langle Q^2 \rangle < 3 \cdot 10^4$ GeV², where the virtual photon radiated from the incoming electron is quasi-real.

The large mass of the c quark provides a "hard" scale needed for the comparison of data to QCD predictions. In leading order (LO) QCD, two types of processes are responsible for charm PHP: Direct photon processes, where the photon interacts as a point-like particle and resolved photon processes, where the photon acts as a source of partons. BGF is the dominant direct photon process. Charm quarks present in the parton distri-

butions of the photon lead to LO resolved charm excitation processes like $cg \rightarrow cg$.

Various NLO calculations exist for comparison with charm HERA data: 1) next-order (FO) approach [1], where only u, d, s are active flavours in the photon and proton; 2) resummed (RS) approach [2,3], where a "massless" c quark is also an active flavour; 3) matched (FONLL) calculation [4], which incorporates mass effects up to NLO and the resummation of p_T logarithms up to next-to-leading logarithm (NLL) level. All these approaches are based on the DGLAP evolution [5]. The CASCADE [6] Monte Carlo (MC), based on the CCFM evolution [7], is a more recent tool to compare with the data.

Charm can be tagged by reconstructing charm mesons via decays such as $D^+ \rightarrow D^0 \pi^+$, $(K^+) \pi^+$, $D^+ \rightarrow K^+ \pi^+$, $D^0 \rightarrow K^+ \pi^-$, $D_s^+ \rightarrow \pi^+ \pi^0$, $(K^+ K^0) \pi^+$, where charge conjugate states are included, or by measuring semileptonic electrons or muons from charm. Reconstructing charm hadrons via their decay vertices with a silicon tracker significantly reduces the background.

2. Inclusive charm meson production

Inclusive production of the charm mesons D^+ , D^0 , D_s and D^+ in DIS has been studied [8] with the H1 detector, using a sample corresponding to an integrated luminosity of 48 pb⁻¹. A

Supported by the Israel Science Foundation and the U.S.-Israel Binational Science Foundation.

silicon tracker separates the production and decay vertices of the pseudoscalar mesons. Differential cross sections have been measured for the D^+ and D^0 mesons and compared with the AROMA [9] LO MC predictions in the kinematic range $2 < Q^2 < 100 \text{ GeV}^2$, $0.05 < y < 0.7$, $p_T(D) > 2.5 \text{ GeV}$ and $|j(D)| < 1.5$, where y is the electron inelasticity and p_T and j are, respectively, the transverse momentum and pseudorapidity of the D meson. j is defined to be positive in the proton beam direction. Results for the D^+ channel are shown in Fig.1. The lower shaded bands indicate the AROMA beauty contribution, scaled by the excess factor of data over MC, as found in the H1 publication [10]. The distributions are well described by the LO QCD simulation, both in normalisation and shape.

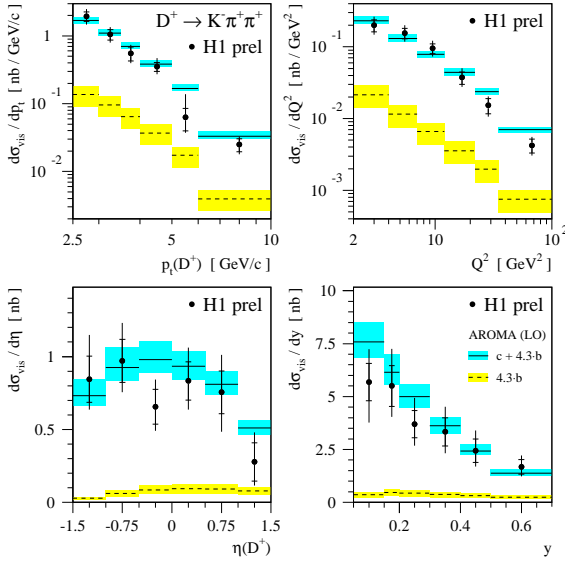


Figure 1. Differential cross sections for D^+ as a function of the D^+ (left) and event (right) variables. The AROMA MC predictions are given by the shaded bands.

Inclusive PHP of D^+ mesons has been measured [11] with the ZEUS detector in the kinematic region $Q^2 < 1 \text{ GeV}^2$, photon-proton centre-of-mass energies $130 < W < 285 \text{ GeV}$,

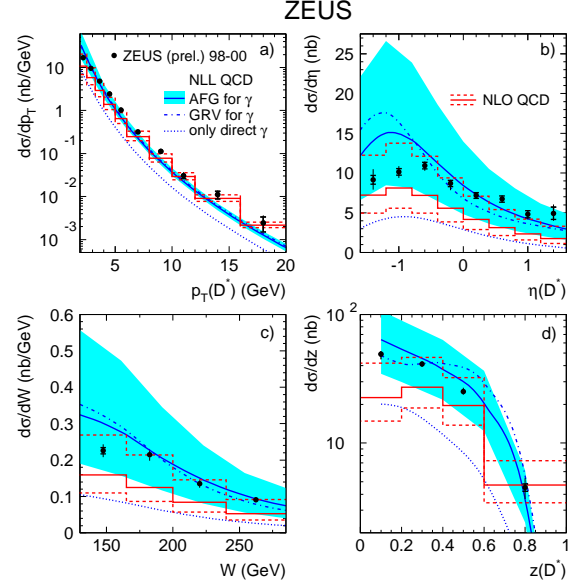


Figure 2. Differential cross sections for inclusive D production as a function of p_T , η , W and z . FO predictions with nominal parameters are given by solid histograms. Upper (lower) dashed histograms correspond to upper (lower) bounds of the predictions. NLL predictions are shown by solid curves and shaded bands (dash-dotted lines) for the AFG (GRV) photon structure function parameterisation. Direct photon NLL predictions are given by the dotted lines.

$1.9 < p_T(D) < 20 \text{ GeV}$ and $|j(D)| < 1.6$, using an integrated luminosity of 79 pb^{-1} . The measured differential cross sections were compared with the NLO predictions FO [1], RS [2] and FONLL [4]. In Fig.2 the distributions $d\sigma/dp_T$, $d\sigma/d\eta$, $d\sigma/dW$ and $d\sigma/dz$ are compared with the FO and RS calculations, where $z(D)$ is the fraction of the photon energy carried by the D meson in the proton rest frame. Theoretical uncertainties obtained by varying the charm mass and renormalisation scale are large, in particular for the NLL predictions. The central FO predictions are below the data, mainly for $\eta > 0$ and low z . The NLL calculations are closer to the data. In particular NLL is better than FO for $d\sigma/dz$ and for $\eta > 0$. A significant resolved contribution

is required in the NLL predictions, which show some sensitivity to the photon structure function parameterisation.

The precise ZEUS data enable measurements of double differential cross sections. In Fig.3 the distributions for four regions in p_T are compared with FO and FONLL predictions. The data is close to the upper band of the predictions and is significantly above the FO and FONLL calculations at medium p_T and positive η , where even the upper bounds are below the data. FONLL predictions are close to the FO ones for low p_T , but below FO for large p_T , where FONLL should do better.

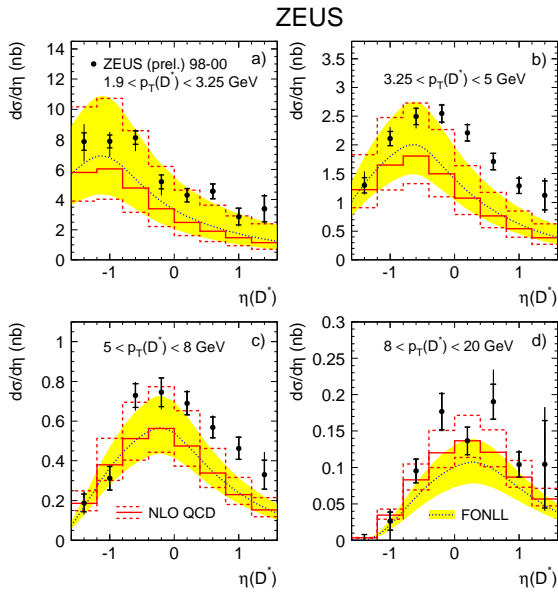


Figure 3. Differential cross sections $d\sigma/d\eta$ for inclusive D production for four p_T regions. FO predictions with nominal parameters are given by solid histograms. Upper (lower) dashed histograms correspond to upper (lower) bounds of the predictions. FONLL predictions are shown as dotted curves with uncertainties given by the shaded bands.

3. Charm dijet angular distributions

Charm-dijet PHP events enable the study of the photon structure, in particular its charm content. Inclusive PHP of D -dijet events has been measured [12] with the ZEUS detector in the kinematic region $Q^2 < 1 \text{ GeV}^2$, $130 < W < 280 \text{ GeV}$, $E_T^{\text{jet}} > 5 \text{ GeV}$, $j^{\text{jet}} j < 2.4$, $M_{jj} > 18 \text{ GeV}$, $j j < 0.7$, $p_t(D) > 3 \text{ GeV}$ and $j(D) j < 1.5$, using an integrated luminosity of 120 pb^{-1} . Here M_{jj} is the jet-jet effective mass and $j j$ is the average pseudorapidity of the two jets. The fraction of the photon momentum producing the two jets is given by: $x^{\text{OBS}} = \frac{j^{\text{jet}} E_T^e}{2yE_e}$. This quantity is close to 1 for direct photons and is less than 1 for resolved photons. A sample of direct- (resolved-)enriched events is defined as $x^{\text{obs}} > 0.75$ (< 0.75).

The differential cross section $d\sigma/dx^{\text{obs}}$ is compared in Fig.4 with LO predictions of the MC program SPYTHIA [13], HERWIG [14] and CASCADE [6] and with NLO FO predictions [1]. A significant contribution (40%) arises from resolved photons. There is a good agreement in shape between the data and the LO MCs, except that CASCADE is too high for the high x^{obs} region. The low x^{obs} tail of the NLO prediction is below the data.

The angle between the jet-jet axis and the beam axis in the dijet rest frame can be approximated by $\cos\theta = \tanh \frac{j^{\text{jet}1} j^{\text{jet}2}}{2}$. In QCD the differential cross section $d\sigma/dj\cos\theta$ is sensitive to the spin of the propagator in the hard subprocess. Whenever the propagator in the LO diagram is a quark, the cross section rises slowly as $(1 - j\cos\theta)^{-1}$, and when it is a gluon, it rises steeply as $(1 - j\cos\theta)^{-2}$.

Fig. 5 shows $d\sigma/dj\cos\theta$ separately for the resolved-enriched ($x^{\text{obs}} < 0.75$) and direct-enriched ($x^{\text{obs}} > 0.75$) samples. The LO MCs SPYTHIA and HERWIG describe the shapes of both data samples. The direct sample rises slowly with $j\cos\theta$, consistent with the q -exchange BGF up-left diagram of Fig.4. The resolved sample rises strongly with $j\cos\theta$ indicating a g -exchange signature. Consequently, the LO subprocess $gg \rightarrow cc$ (up-right diagram of Fig.4) can-

not dominate the resolved photon charm-dijet process. This suggests the dominance of the LO charm-excitation process of $\gamma^* \rightarrow c\bar{c}$ (down-right diagram of g.4).

The two jets can be distinguished by associating the D meson to the closest jet in η space. Calling this "D-jet" jet 1, the $d = d \cos \theta_{\text{rise}}$ can be studied separately for the photon and proton directions. Fig. 7 shows the differential cross sections as a function of $\cos \theta_{\text{rise}}$ for the resolved- and direct-enriched samples. The PYTHIA estimation of the resolved process contribution to the direct-enriched sample (g.7b) explains the asymmetric distribution in $\cos \theta_{\text{rise}}$. The strong rise in $d = d \cos \theta_{\text{rise}}$ towards the photon direction for the resolved-enriched sample is clear evidence for charm from the photon in the LO picture. The NLO FO predictions describe the data well for $x^{\text{obs}} > 0.75$ (g.7d), but are below the data for $x^{\text{obs}} < 0.75$ (g.7c), both for the proton and photon directions. The data shapes are reproduced. The CASCADE predictions exceed the data by 30%, mostly for $x^{\text{obs}} > 0.75$. A gain the shapes are reasonably well reproduced.

4. Charm fragmentation

Charm quark hadronisation into charm mesons is parametrised by fragmentation functions, which exist in many forms with tunable parameters fixed from ts to e^+e^- data. A direct measurement of the fragmentation function at HERA can reduce theoretical uncertainties and test the universality of charm fragmentation.

Charm-jet PHP events have been measured [15] with the ZEUS detector, using an integrated luminosity of 120 pb^{-1} , in the kinematic region $Q^2 < 1 \text{ GeV}^2$, $130 < W < 280 \text{ GeV}$. At least one jet had to satisfy $E_T^{\text{jet}} > 9 \text{ GeV}$, $j^{\text{jet}} < 2.4$ and a D meson with $p_T(D) > 2 \text{ GeV}$, $j(D) < 1.5$ had to be associated with a jet. The fraction of jet energy carried by the D was defined as $z = \frac{(E + p_x)_D}{2E_{\text{jet}}}$, where p_x is the D longitudinal momentum relative to the jet axis. The normalised differential cross section in z was compared to the PYTHIA LO MC with the Peterson fragmentation function [16] $f(z) / [z(1-z)^2]^{-1}$, for various

values of the free parameter α . Strong sensitivity to the α value was found. A fit to the best value yielded $\alpha = 0.064 \pm 0.006^{+0.011}_{-0.008}$, compared to 0.053 from LO fits to the LEP data.

The z distribution measured with the ZEUS data was compared to that from e^+e^- colliders, where z was defined as $z = E_D / E_{\text{beam}}$. The comparison with OPAL and ARGUS results is shown in g. 6. Similar shapes are obtained for $z > 0.3$ with precision of the HERA data competitive with the LEP data. The low- z peak in the OPAL data is due to gluon splitting to $c\bar{c}$. The results support the universality of the charm fragmentation function.

The H1 measurements [8] of inclusive charm mesons in the DIS regime (section 2) were used to deduce preliminary fragmentation fractions of the charm quark to the various mesons. The results, compared with the e^+e^- world average values (in brackets), are:

$$\begin{aligned} f(c \rightarrow D^+) &= 0.20 \pm 0.02^{+0.04+0.03}_{-0.03-0.02} \quad (0.23 \pm 0.02) \\ f(c \rightarrow D^0) &= 0.66 \pm 0.05^{+0.12+0.09}_{-0.14-0.05} \quad (0.55 \pm 0.03) \\ f(c \rightarrow D_s^+) &= 0.16 \pm 0.04^{+0.04+0.05}_{-0.04-0.05} \quad (0.10 \pm 0.03) \\ f(c \rightarrow D^*) &= 0.26 \pm 0.02^{+0.06+0.03}_{-0.04-0.02} \quad (0.24 \pm 0.01) \end{aligned}$$

where the first uncertainty is statistical, the second is systematic and the third is from theory.

In addition, the H1 measured cross sections were used to test the isospin invariance of the fragmentation process by calculating the ratio of neutral (cu) to charged (cd) D-meson production

$$R_{u=d} = \frac{d\sigma(D^0) + d\sigma(D^-)}{d\sigma(D^+) + d\sigma(D^*)} = \frac{(D^0) + (D^*) BR}{(D^+) + (D^-) BR}$$

and to extract the strangeness suppression factor

$$r_s = \frac{2f(c \rightarrow D_s^+)}{f(c \rightarrow D^+) + f(c \rightarrow D^0)}$$

and the fraction of D mesons produced in a vector state $P_V = \frac{V}{V+P+S} = \frac{D}{D+D^*}$. Here $BR = 0.677 \pm 0.005$

is the $D^+ \rightarrow D^0 + \pi^+$ branching ratio. The results, compared with previous values, are:

$$\begin{aligned} R_{u=d} &= 1.26 \pm 0.20 \pm 0.12 \quad (\text{H1 prel.}) \\ &1.00 \pm 0.09 \quad (e^+e^- \text{ world average}) \\ r_s &= 0.36 \pm 0.10 \pm 0.08 \quad (\text{H1 prel.}) \\ &0.27 \pm 0.04 \pm 0.03 \quad (\text{ZEUS}) \\ &0.26 \pm 0.03 \quad (e^+e^- \text{ world average}) \\ P_V &= 0.69 \pm 0.04 \pm 0.01 \quad (\text{H1 prel.}) \\ &0.55 \pm 0.04 \pm 0.03 \quad (\text{ZEUS prel.}) \\ &0.60 \pm 0.03 \quad (e^+e^- \text{ world average}). \end{aligned}$$

All the HERA measurements are in good agree-

ment with e^+e^- world average results, indicating again the universality of charm fragmentation.

REFERENCES

1. S. Frixione et al., Nucl. Phys. B 412 (1994) 225; Phys. Lett. B 348 (1995) 633; Nucl. Phys. B 454 (1995) 3.
2. B. A. Kniehl et al., Z. Phys. C 76 (1997) 689; J. Binnewies et al., Z. Phys. C 76 (1997) 677; Phys. Rev. D 58 (1998) 014014.
3. M. Cacciari et al., Phys. Rev. D 55 (1997) 2736, 7134.
4. M. Cacciari et al., JHEP 0103 (2001) 6.
5. V. N. Gribov et al., Sov. J. Nucl. Phys. 15 (1972) 438; L. N. Lipatov, Sov. J. Nucl. Phys. 20 (1975) 94; G. Altarelli et al., Nucl. Phys. B 126 (1977) 298; Yu. L. Dokshitzer, Sov. Phys. JETP 46 (1977) 641.
6. H. Jung et al., Eur. Phys. J. C 19 (2001) 351; H. Jung, Comput. Phys. Commun. 143 (2002) 100; J. Phys. G 28 (2002) 971.
7. M. Ciaffaboni, Nucl. Phys. B 296 (1988) 49; S. Catani et al., Phys. Lett. B 234 (1990) 339; Nucl. Phys. B 336 (1990) 18; G. Marchesini, Nucl. Phys. B 445 (1995) 49.
8. H1 Collaboration, paper 1015 submitted to the Int. Conf. on High Energy Physics, ICHEP2002, Amsterdam.
9. G. Ingemann et al., Comput. Phys. Commun. 101 (1997) 135.
10. H1 Collaboration, S. Aid et al., Phys. Lett. B 467 (1999) 156.
11. ZEUS Collaboration, paper 786 submitted to the Int. Conf. on High Energy Physics, ICHEP2002, Amsterdam.
12. ZEUS Collaboration, S. Chekanov et al., DESY 03-015 preprint and hep-ex/0302025, Phys. Lett. B (2003) in print.
13. T. Sjöstrand, Comput. Phys. Commun. 82 (1994) 74.
14. G. Marchesini et al., Comput. Phys. Commun. 67 (1992) 465.
15. ZEUS Collaboration, paper 778 submitted to the Int. Conf. on High Energy Physics, ICHEP2002, Amsterdam.
16. C. Peterson et al., Phys. Rev. D 27 (1983) 105.

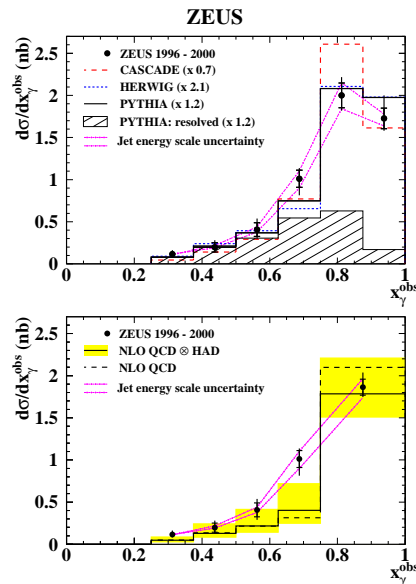
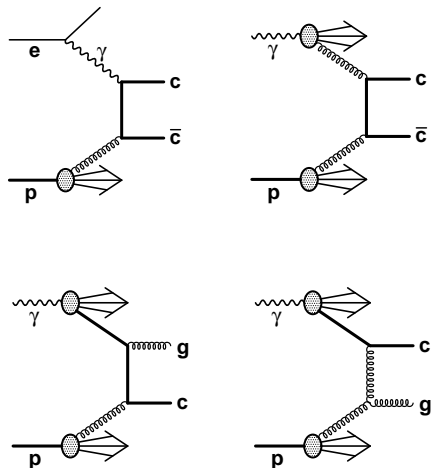


Figure 4. Upper part: LO QCD charm-production diagrams. Direct photon, BGF ($g!cc$); resolved photon ($gg!cc$); resolved-photon charm excitation ($cg!gc$, c in proton hemisphere); resolved-photon charm excitation ($cg!cg$, c in photon hemisphere). Lower part: Differential cross-section $d\sigma/dx_{\gamma}^{obs}$ for the data compared with MC simulations (upper plot) and NLO FO predictions (lower plot). Each MC distribution is normalised to the data, as indicated in the brackets. The NLO uncertainty after hadronisation is given by the shaded band.

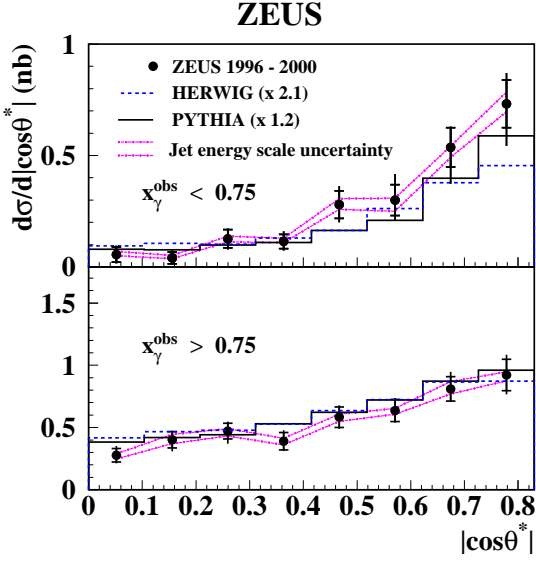


Figure 5. Differential cross sections $d\sigma/d|\cos\theta^*|$ compared with MC simulations for samples enriched in resolved- (upper plot) and direct- (lower plot) photon events.

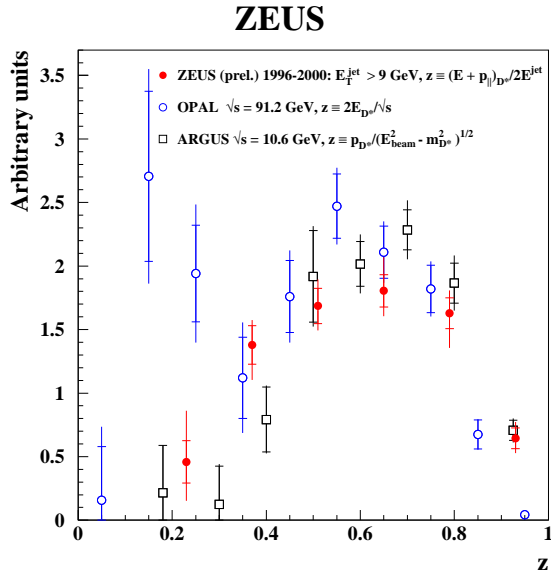


Figure 6. Fragmentation function versus z for the ZEUS data compared to e^+e^- measurements. The data sets were normalised to $1/(\text{bin width})$ for $z > 0.3$.

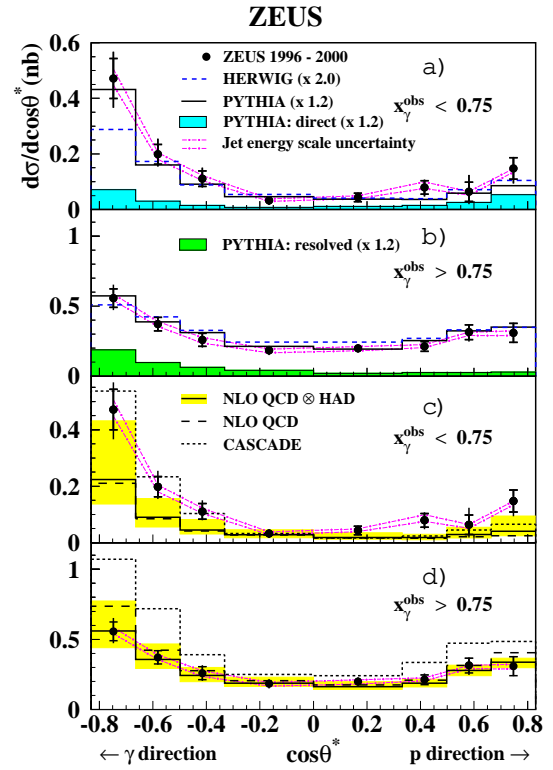


Figure 7. Differential cross sections $d\sigma/d\cos\theta^*$ compared with MC simulations and NLO FO predictions for samples enriched in resolved- (a,c) and direct- (b,d) photon events. The shaded areas in (a,b) are the contribution of the PYTHIA direct photon process to the resolved-enriched sample and of the resolved photon process to the direct-enriched sample, respectively. The NLO uncertainty after hadronisation is given by the shaded band.